EVENTS SELECTION,EFFICIENCY OF REGISTRATION AND CALCULATION OF THE SIZE SPECTRA CORRECTIONS FOR MAKET-ANI INSTALLATION

S.Sokhoyan *

Yerevan Physics Institute, Cosmic Ray Division, Armenia.

1 Introduction

Extensive air showers (EAS) are produced at Primary Cosmic Ray (PCR) strong interactions with nuclei of air atoms. Decay of secondary π^0 and η-mezons initiate electron-photon, and charge pions, kaons etc. - muon and neutrino components of secondary cosmic rays.

Electron-photon cascade generated in this case at energies $E_0 \sim 10^6$ Gev have mean square radius $\sim 70m$ at sea level, but total size composes hundreds of metres [1].

Large lateral sizes give possibility of EAS registration by small number of spreaded detectors covering large surfaces and simultaneously dictate the topography of EAS investigated installations at given atmospheric depth.

The majority of up today well known facilities [2], [3], [4], [6], [8], [7] orientated on the investigations of the size spectra "knee" region investigations have dimensions $\sim$ 100m and registered particles number $10^4 < N_e < 10^7$. Density of detectors arrangement is maximum in the centre of the installations and decreases moving towards to the periphery. In triggering conditions decisive role also as a rule carry detectors of central part of installation.

For reliable reconstruction of the CR flux incident on the atmosphere it is necessary to investigate efficiency of registration as function on EAS core distance from the centre of the installation and distortions of the shower parameters such as particles number N_e, age s and incidence zenith angle θ.

The data on efficiency of registration for different installations known from references could devide on three groups.

I. As effective area S_{eff} considered surface within which satisfaction of triggering conditions for $\sim 100\%$ events in region above threshold of registration $N_e > N_e{}^{(thr)}$(or $E > E^{(thr)}$) independently on core distance from centre of installation, particles number, age and incidence zenith angle is observed.

Determination of S_{eff} by this way was done, for example, on installations [2], [3], [4], [6].

TIBET experiment[2].

Array of Tibet experiment installation is covered area $S_{tot} \approx 15000m^2$. One from main conditions of events selection is: the core position of each shower should be inside the innermost 5 x 5 detectors, or their co-ordinates $X \leq 30m$ and $Y \leq 30m$. Within this area satisfaction of triggering conditions($E^{(thr)} = 10^{14}eV; \theta < 25^o$) for $\approx 100\%$ events independently on EAS energy is observed. Thus: $S_{tot}/S_{eff} \approx 4$.

*corresponding author: e-mail: serg@crdlx5.yerphi.am

KASCADE experiment[3].

For the detection of the electron component of an EAS the KASCADE experiment uses $200\times200m^2$ scintillator array. For showers with $N_e > 3 \times 10^4$ and with cores inside 91 m from centre of the array the efficiency of registration is independent from the core position and is larger than 95%. Therefore, $S_{tot}/S_{eff} \approx 1.5$

.

E A S - T O P experiment[4].

The trigger efficiency has been studied by simulating the array response as a function of zenith angle θ and shower size(including all experimental dispersions and triggering conditions). Then determined fixed area where triggering efficiency is greater than 95% for $N_e > 10^{5.2}$, independent on θ(for $\theta < 40^o$). At further analysis fluxes are corrected for the calculated triggering efficiency.
For this experiment $S_{tot}/S_{eff} \approx 3.5$.

T I E N - S H A N experiment[6].

For all $N_e > 5.6 * 10^5$ and $\theta < 30^0$ circle with radius R=18m as effective area was considered[5]. The installation registeres such showers with efficiency $\varepsilon > 90\%$. With account only central part of scintillator array for this installation $S_{tot}/S_{eff} \approx 2$.
The value of S_{tot}/S_{eff} relation depend from density of array detecors arrangement and triggering conditions of concrete installation.

As it is evidently lack of this method of events selection is essential decrease of EAS axes gathering surface by cause of low efficiencies of registration for low energy showers hiting array of installation outside of found areas. At the same time essential part of high-energy showers effectively registered outside found effective area is lossed. It's very important for statistically poor EAS investigating installations especially in region above "knee" of the size spectra($N_e > 10^6$).
Moreover, this method assumed independence of registration efficiency on age parameter within found effective area.

II. Effective area of registration is function on shower size N_e.
For any $N_e > N_e^i$(where N_e^i are some fixed values of shower size) areas with high registration efficiency are determined.

M A K E T - A N I experiment[7].

Preliminary results [7] of size spectra investigations by MAKET-ANI installation data were obtained by this way. By simulating data constancy of events number per unit area(fluxes) at different core distances from centre of installation and fixed values of N_e^i was traced. Parallel constancy of the size spectra shape(slopes, knee position) at these conditions was traced also and thus effective area as function of N_e was found. This method also assumed independence of effective area of registration from age value.
However, absence of account of registration efficiency dependences on s and N_e by these two methods may essentially distort reconstructed size spectrum and age parameter distribution and calls in question reliability of spectra shape.

III. Total registration area is examined by correlating the co-ordinates of individual shower core X_0, Y_0 and parameters N_e, s and θ . The goal is to outline regions with constant densities of events number ρ_{stat} [8],[9]. So, efficiency of registration consider as four-dimensional function of N_e, s, r

and θ.

AKENO experiment[8].

In constructing the size spectrum the showers whose cores hit the area of 100% detection efficiency are selected. This area is determined by plotting the core positions on the map in each size, zenith angle and age bin and then selecting the region where the cores are distributed uniformly.
In the basis of our investigations and determination of effective detection areas for MAKET ANI installation lie last method with some differences.
All surface of array was devide on belts. It is necessary to note that the majority of EAS installations are simmetric - detectors are located on concentric circles[11] around centre of installation. MAKET ANI installation differed from all these installations and extend on length. It is reason that we use not concentric circles, but belts(see Fig.1) with fixed co-ordinates steps: along oX axis ΔX = 4m, but along oY axis ΔY = 2m.

2 Algorithm of Monte - Carlo simulation

The sequence of the data acqusition and its final processing are identical on the majority of the EAS installations. First of all it is forming of the raw data "zero" bank, where information from amplitude detectors(in codes), information from timing detectors using further for zenith and azimuth angles determination, astronomical time of each event etc., are stored. Moreover, in Zero Data Bank of MAKET ANI installation, for example, some results of on-line processing are stored also. These are: global intensity of showers hiting area of installation, intensity of events, background spectra and their slopes by each detector data. Main parameters of individual showers (electron number N_e, co-ordinates of the shower axis X_0, Y_0 , age parameter s, angles θ and φ are stored in the Primary Data Bank.

Determination of the mentioned EAS parameters on the majority of installations is carried out by fitting the particle densities measured by detectors to the NKG-formula[10].
In the Secondary Data Bank experimental events corresponding to the registration efficiency of about 100% are stored.
For the determination of effective areas of registration as a rule simulated data banks are applied and then obtained values are used at the Secondary Experimental Data Bank selection.
For simulation of response function of installation simple EAS "generator" simulating experimental situation on the observation level was used[12].

Well known NKG-approximation of EAS electron-photon component [10] in approach[12],[13] was used:

$$\rho(r_i) = \frac{N_e}{{r_m}^2} * \left(\frac{r_i}{r_m}\right)^{0.18} * 0.366 * C(s) * \left(\frac{r_i}{r_m}\right)^{(s-2)} \left(\frac{r_i}{r_m} + 1\right)^{(s-4.5)} \quad (1)$$

where $\rho(r_i)$ - densities measured by scintillation detectors, $r_m = 121m-$ value of Molier radius corresponding Aragads level(3200m a.s.l.)

Simulation of showers is carried out in the following sequence.
1. On the rectangular surface with sizes $|X_{max}| = 60m$ and $|Y_{max}| = 30m$ the EAS axes are uniformly simulated .
2. N_e values are simulated assuming power law of EAS without "knee" and with slope $\gamma = -2.5$, age s is simulated by Gaussian distribution around average value $< s >= 1.055$ with $\sigma = 0.2 * < s >$. Threshold on particles number is ${N_e}^{(thr)} = 3 * 10^4$.

3. Zenith angle of incidence θ is simulated according to distribution $cos^{5.4}\theta$ within $0^\circ < \theta < 60^\circ$, and azimuth angle φ - uniformly within $0 < \varphi < 2\pi$.
4. Distances of detectors from EAS axis are determined, local densities ρ_i are calculated by formula (1).
5. The particles number in the individual detector is determined by:

$$N_e{}^{(i)} = \rho_i * S_i, \tag{2}$$

where S_i - is the surface of the detector.
6. Fluctuations of calculated local $N_e{}^{(i)}$, of the loss of the energy in scintillator, of the collection of light in phototubes etc. are introduced. Detail description of these procedures is given in [12],[14].
7. Conversion to "experimental" codes.
8. Execution of installation triggering conditions(also see [12]).

Then procedures of each showers parameters reconstruction are started.
1. Conversion from codes to the particles number.
2. Density at each detector and further average density at fixed core distance are determined.
3. Fitted discrete function ρ_i by NKG-function.
4. Determination of N_e and s.

2.1 Organization of Monte-Carlo simulated bank

Simulation of events was carried out in two stages.

FIRST STAGE

1. Interval $5 * 10^4 < N_e < 10^7$ is devided uniformly(in logarithmic scale) into 30 bins;
2. Ages range $0 \div 2$ is divided into 15 bins;
3. Number of belt n_{belt} is fixed ;
4. Simulate at given N_e of 5000 events for 15 values of age by above described algorithm;
5. Check of triggering conditions for each from these 5000 simulated events and in case of satisfaction them this event is stored;
6. Calculate efficiency of registration as ratio of "survived" to total number of events at given values of N_e and s;
7. Number of N_e is changed and procedures $4 \div 7$ are carried out for all energies;
8. Number of belt is increased and procedures $3 \div 7$ are carried out for belts $1 \div 12$.

The results of the first stage are stored as tables(presented in Fig.2,3) where efficiencies of registration as functions on age parameter for nine fixed values of N_e in each from 12 belts are shown. From these figures it is possible to come the following conclusions:
- all showers with $N_e > 10^6$(independently on s) are registered with high efficiency($\varepsilon \gtrsim 90\%$) up to belts $(19 \times 38) \div (21 \times 42)$, that is corresponded to $n_{belt} = 10$;
- in belt 11 are effectively registered only EAS with $N_e > 3 * 10^6$ and "young" ages($0.3 < s < 0.8$) ;
- at belts $> (23 \times 46)$ m high efficiency is not observed at any N_e;
- "mature" ages ($0.8 < s < 1.2$) are effectively registered for all $N_e > 5 * 10^4$ up to (7×14) belts ($n_{belt} = 1 \div 3$);
- at larger belts "mature" ages are effectively registered for all $N_e > 2 * 10^5$ up to (15×30) belts ($n_{belt} = 7$);

- at $(11 \times 22) \div (15 \times 30)$ belts ($n_{belt} = 6 \div 8$) in the "mature" range of ages only $N_e > 10^5$ are effectively registered;
- at $(17 \times 34) \div (19 \times 38)$ belt ($n_{belt} = 9$) in the "mature" range of ages only $N_e > 10^6$ are effectively registered;
- at $(19 \times 38) \div (21 \times 42)$ belt$(n_{belt} = 10) \longrightarrow N_e > 2 * 10^6$;
-"young" ($0.3 < s < 0.8$) and "old" ages behave practical simmetrically up to belts 19×38;
- at belts $\geq 19 \times 38$ asimmetry in the $\varepsilon(s)$ function form appears.

From Fig.3 becomes clear reason of selection as maximum acceptable belt $n_{belt} = 12$: registration efficiency ($\varepsilon \gtrsim 80\%$) is observed here only at maximum values of electrons number $N_e \sim 10^7$ and "ypung" ages. In the next belts high efficiency is not observed at any N_e value.

SECOND STAGE

By above described simulation $3 * 10^6$ events satisfacting the triggering conditions were simulated (Primary M-C Data Bank) and then data processing is started. First of all events were selected by the selection criteria identical to experimental ones:
1. Shower co-ordinates determination errors $\delta_{|x|} \leq 4.5$ m and $\delta_{|y|} \leq 4.5$ m.
2. Age parameter determination errors $\delta_s{}^{(rec)} \leq 0.45$.
3. Value of χ^2-parameter of reconstruction $\chi^2 < 3.5$.
4. $0.3 < s^{(rec)} < 1.7$

Events satisfacting to these conditions were stored in the Secondary M-C Data Bank.
And, finally events selection according to registration efficiencies is performed:
-threshold on $N_e \geq 5 * 10^4$ is established.
-the belt number is determined by the shower axis co-ordinates;
-for estimated N_e and s values efficiency of registration for the given belt is determined from tables. In case if this value is larger than given ε threshold value, then event in Third M-C Data Bank is stored.
The investigations given below are carried out in main at efficiency threshold value $\varepsilon_{thr} = 90\%$. Moreover, all results obtained by the Primary M-C Data Bank are marked with index ($trig$), in the Secondary M-C Data Bank - with index (rec), and in the Third M-C Data Bank - with index (eff).

3 Errors of EAS parameters determination

As essential part of simulating data is not satisfy triggering conditions "conjunction" of individual showers parameters reconstructed values with primary M-C data is not possible. Because of that as a standard of comparison parameters of showers satisfacting to triggering conditions were taken. These values of parameters are of course coincided with primary M-C data for this event. Certainly events selectance by trigger may be distort both age parameter distribution and size spectrum. It is also illustrated below.
Nevertheless reliability of errors determination procedure is ensured here. As to size spectrum and age distribution but they finally obtained by above mentioned procedure (see p3.1) will be compared with "true" analitically tractable size spectrum and age distribution.

3.1 Errors of shower axis co-ordinates reconstruction.

For determination of co-ordinates reconstruction errors, and possible misclassification of the "true" belt number, for each event "true" fixed values of axis co-ordinates X_0,Y_0 and reconstructed values ${X_0}^{(rec)}$ and ${Y_0}^{(rec)}$ are stored. The distributions of event number obtained for each belt is constructed. The same procedure was carried out with account of registration efficiency $\varepsilon \geq 90\%$ and results are shown in Fig.4. As orientir of the belt on oX axis here and below belt surface is indicated(instead of distance r from installation centre as it would be in the case of simmetric installation). On the oY axis fraction of the reconstructed events is plotted. As it is seen from Fig.4 accuracy of shower axis co-ordinates determination in first five belts constitutes $\approx 80-90\%$ and then it is declined with increasing of belt number to $\approx 50-55\%$ in last two belts. From this figure it is also seen that reconstruction of shower axis co-ordinates with account of registration efficiency improves situation: accuracy of shower axis co-ordinates determination in first 5 belts is increases to $85-90\%$, in 7 and 8 belts it is equal to $\approx 75-80\%$. Though the improvement in last three belts is observed also, accuracy of co-ordinates determination here is less than 65%. It means that both behaviour of age and size spectrum in these belts is distorted essentially. The reason of it becomes understandable from Fig.1 where practical absence of detectors in the last four belts is seen that brings to large errors of shower axis determination.

3.2 Errors of EAS age parameter determination

In Fig.5,6 $s^{(rec)}$ and $s_{eff}^{(rec)}$ ages distributions are compared with "true" M-C distributions for all 10 belts. In Fig.7 age distributions within all examined area (Fig.7(a)), average values of age as function on belt number(Fig.7(b)) and standard deviation of age distributions in belts (Fig.7(c)) are shown. As it is seen from Fig.5, though average values of age distribution reconstructed without account of registration efficiency practically are coincied with "true" values (Fig.7(b)) within all 10 belts, but values of standard deviation are essentially greater than "true" values (Fig.7(c)). At the same time average values of age distributions obtained at $\varepsilon \geq 90\%$ are sistematically shifted to left ($\delta s \approx 0.06$), but dispersions of their are practically coincied with "true" values. Data of Fig.7(a) may be used for the correction of age parameter distribution obtained over all area of installation.

3.3 Errors of EAS size determination

In Fig.8,9 distributions of the value ${N_e}^{(rec)}/{N_e}^{(trig)}$ for events after reconstruction of shower parameters and after supplementar events selection by the efficiencies of registration are shown. In Fig.10 average values of distributions $\Delta N_e/{N_e}^{(trig)} >$ for each belt are shown. As it is seen from Fig.8 average $< {N_e}^{(rec)}/{N_e}^{(trig)} >$ within first 6 belts are shifted concerning "true" values from 5 to 15% and the last value is practically constant up to belt 10. However, as it is seen from Fig.9 essential increasing of standard deviation σ for these distributions from 0.18 to 0.35 within first 6 belts is observed. Then this value is slowly decresed to 0.30 in belt 10. As it is seen from Fig.8,9 values of $< {N_e}^{(rec)}/{N_e}^{(trig)} >$ distributions for data obtained at $\varepsilon \geq 90\%$ are essentially smaller and practical doesn't change with belts number. As to average values maximum deviation from "true" as it is seen from Fig.10 a) is less than 5% but standard deviation (Fig.10 b)) of N_e errors distributions $\Delta N_e/{N_e}^{(trig)} >$ is not changed within all 10 belts($\sigma \approx 0.1$).

4 Differential size spectra in belts

In Fig.11,12 differential size spectra in belts after execution of triggering conditions, EAS parameters reconstruction and after reconstruction at $\varepsilon \geq 90\%$ are shown. Spectra are normalized on corresponding belts surfaces and are multiplied by ${N_e}^{2.5}$. As it is seen from these figures "threshold" region of the last variant spectrum is shifted to right with moving to periphery. It may be explained that at larger distances more effectively large N_e are registered. Term "threshold" region is used here because tuning of threshold on efficiency is similar to threshold tuning on particles number (see Fig.2,3). Nonlinearity of spectrum in the threshold regions is explained by transferings to larger N_e. Following peculiarities of spectra are also evident:
-intensity of "reconstructed" spectrum within first seven belts exceed intensity of "true" spectrum in range $10^5 < N_e < 4 * 10^5$. The reason of this excess are probably transferings to larger N_e also. By steeper character of spectrum number of the such transferings is larger than transferings to small N_e;
-violation of spectrum intensity constancy within last three belts is observed. It may bring to nonlinearity of size spectrum front part constructed by data of all 12 belts.

4.1 Size spectrum corrections

Two variants of spectrum construction using simulated events from total area (10 belts) were used.
1. Parallel with size spectra construction in belts carry out the summation of each event in general spectrum for all area.
2. For each pair N_e and s, values for individual event maximum possible value of area with efficiency of registration larger that given threshold ε_{thr} by efficiencies tables (see Fig.2, 3) is found. Found value of the surface is introduced in averaging procedure. The general spectrum is normalized on such average value of effective area of registration. The spectrum obtained in result of this procedure, "triggering" spectrum and "reconstructed" spectrum also in comparison with "true" M-C spectrum are shown in Fig.13(b). As it was expected "triggering" and "reconstructing" spectra have evident non-linearity in region up to $N_e = 10^6$.
However, spectrum constructed with account of registration efficiency is practically coincided with M-C spectrum starting from $N_e = 1.2 * 10^5$. In Fig.13(c) relations of intensities of all three spectra variants to "true" intensities(correction coefficients) are shown. As it is seen from Fig.13(b) "triggering" and "reconstructing" spectra are essentially differed from "true" spectrum.
Errors of N_e determination $\delta N_e / {N_e}^{(trig)}$ for (rec) and (rec) at $\varepsilon \geq 90\%$ variants are shown in Fig.13(a) and confirm behaviour of these values in belts (see Fig.10). For the check of expected coincidence of "reconstructing" and M-C spectra in the central part of installation, corresponding general spectra within first 6 belts were constructed and are shown in Fig.14. From this figure it is seen that situation is principle changed (value of correction coefficients ~ 1). However, it is evident that essential part of statistics of showers with co-ordinates of axis outside the first 6 belts in this case is lossed.

5 Statistics

One of the goals of presented work was increasing of selected experimental events, especially in region of spectrum above "knee" $N_e > 10^6$ and of course final distribution of statistics for all three variants of events selection is important. Moreover, this analysis was carried out at other two threshold values of registration efficiency ($\varepsilon_{thr} = 80\%$ and $\varepsilon_{thr} = 85\%$) too. Results of this analysis are shown in Fig.15, from where it is seen that full statistics in first 3-4 belts for all three thresholds of efficiency is practically constant. At moving to periphery with account of registration efficiency essentiall part of statistics is lossed and as it is shown below(Fig.16) are lossed in main showers with

size $N_e < 10^6$. Changing of efficiency threshold, of course, reflects on corrections coefficients for size spectra and age distribution and is not principle at least for high efficiencies. In other hand decreasing of threshold value of efficiency to ($\varepsilon_{thr} = 80\%$ make possible of using statistics of belts 11 and 12, where satisfacting of triggering conditions at $N_e! > 10^6$ and ages $0.3 < s < 1$ with such efficiency is observed (see Fig.2,3). In Fig.16 is shown distribution of statistics in belts for range $N_e > 10^6$. As it is seen from figure statictics increased linearly with belt number(up to belt 10) and is independ from data selection method. Once more it confirms that at registration efficiency threshold $\varepsilon \geq 90\%$ statistics is lossed at range $N_e < 10^6$ only.

References

[1] Murzin V.S., *Introduction to Cosmic Rays Physics*, Atomizdat, 1979

[2] M.Amenomori et.al.*The Astrophys.J.*,v.461,1,part 1,1996.

[3] R.Glasstetter for the KASCADE collaboration, Proc. 25th ICRC (Durban, 1997), vol. 2.

[4] Aglietta M. et. al. *Astropart. Phys.,10,(1999) 1.*

[5] Adamov D.S. Ph.D.Thesis, Moscow,1990.

[6] Danilova E.V. et.al., Proc. 24th ICRC (Rom, 1995), vol. 1, 285

[7] Chilingarian A. et al., Proc. 26th ICRC (Salt Lake City, 1999), **1**, *240*

[8] Nagano M., et. al., 1984, J. Phys. G, **10**, *27*

[9] Hayakawa S., Cosmic Ray Physics, Intersience Monographs and Texts in Physics and Astronomy, V. 22, Wiley-Interscience, 1969.

[10] Nishimura J., Handbuch der Physik, Bd. XLVI/2,Berlin,1967,S.1. Astronomy, V. 22, Wiley-Interscience, 1969

[11] Khristiansen G.B. et al., Cosmic Rays of Superhigh Energies (in Russian), Atomizdat, 1975, 27

[12] Hovsepyan G.G. Report for the ANI collaboration.,March-2000,Yerewan.
Blokhin S.V., Romakhin V.A., Hovsepyan G.G., Proc. Workshop ANI 99, (Nor-Amberd, 1999).

[13] V.S.Aseikin et.al. Lebedev Inst. Proc.,109,1979,v.3, Moscow(in Russian)

[14] Hovsepyan G.G. for the ANI collaboration., Proc. Workshop ANI 98, FZKA 6215, (Nor-Amberd, 1998).

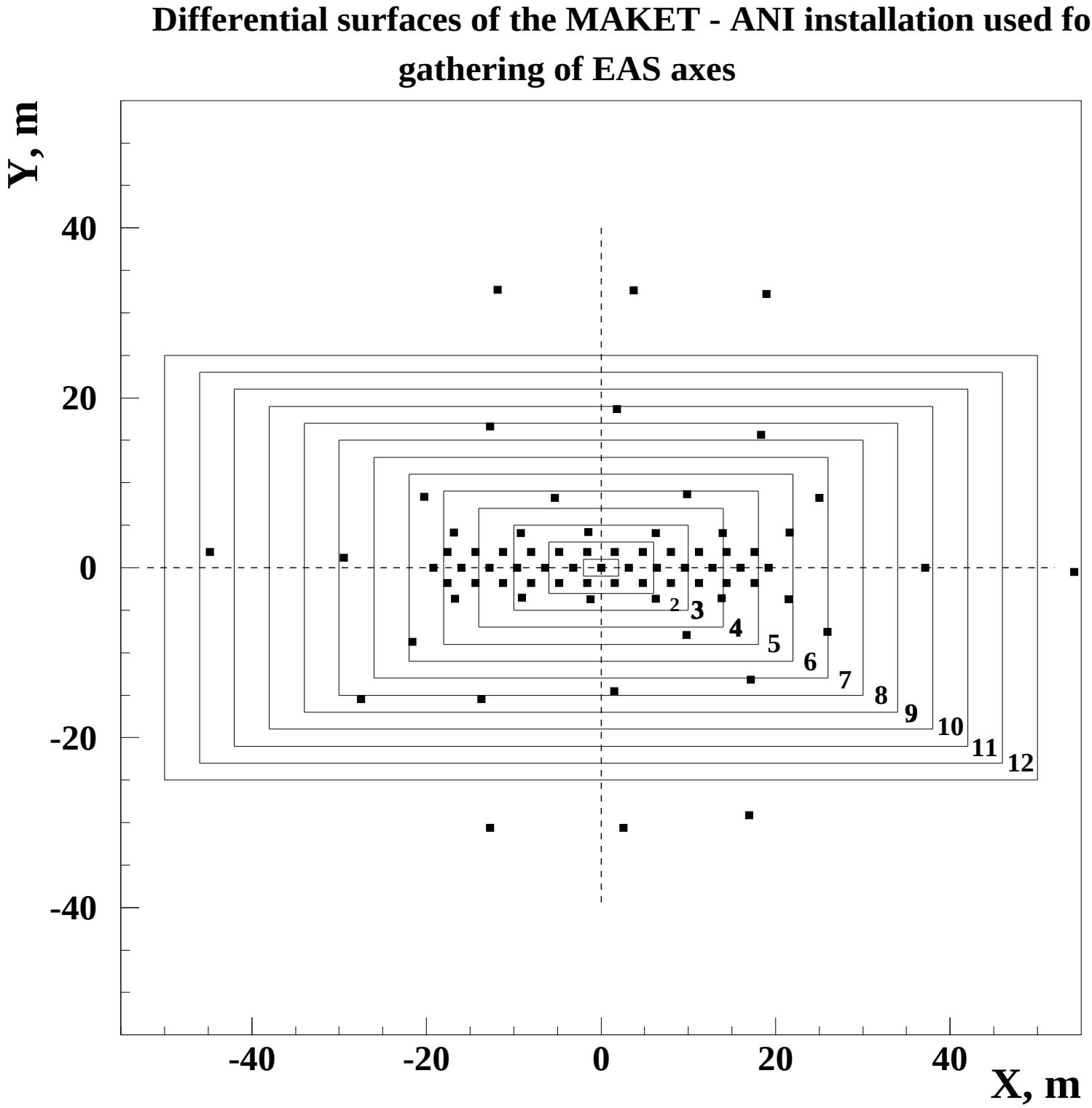
Differential surfaces of the MAKET - ANI installation used for gathering of EAS axes
Y, m
40
20
0
-20
-40
-40
-20
0
20
40
X, m
2
3
4
5
6
7
8
9
10
11
12

Figure 1:

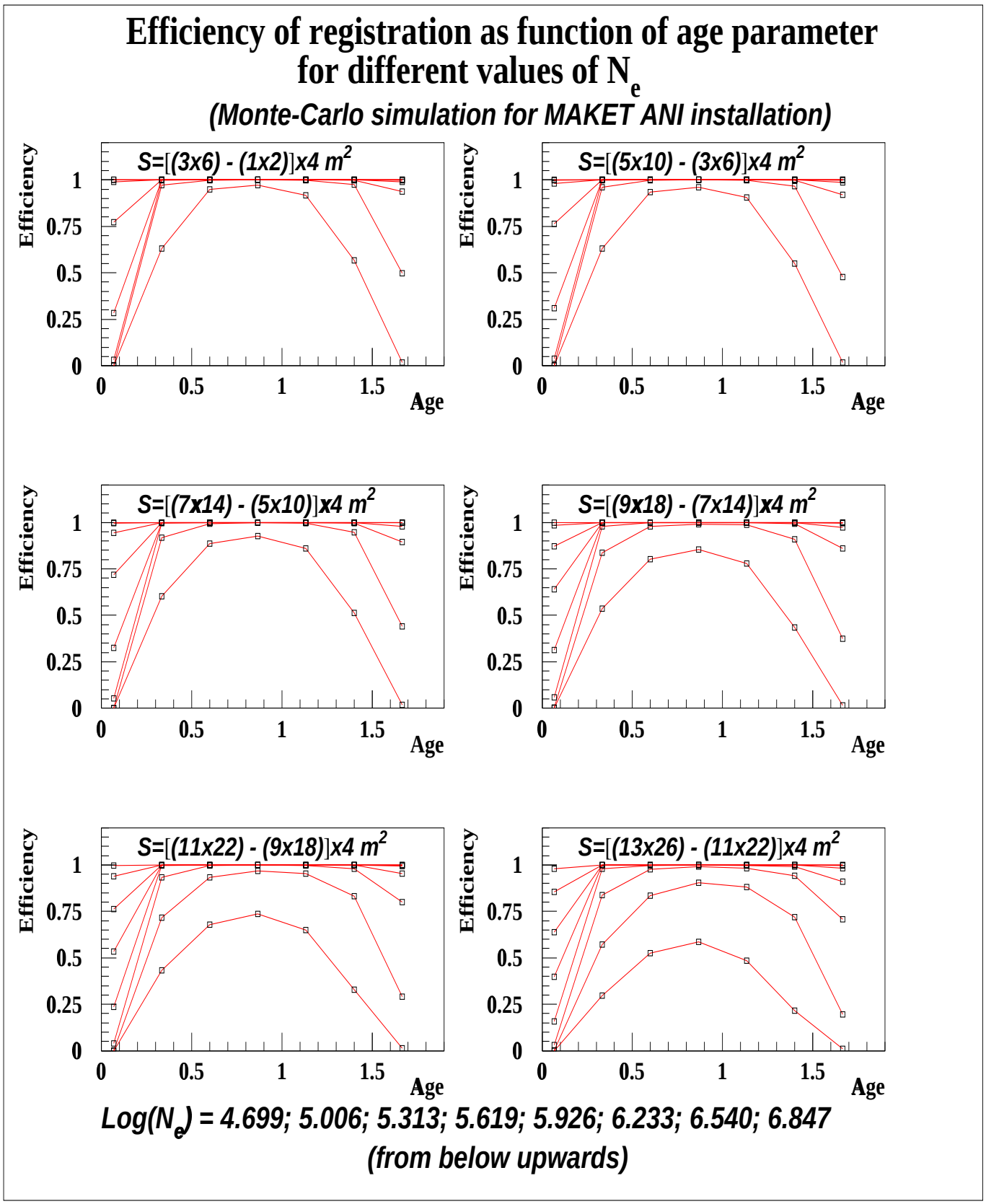
Efficiency of registration as function of age parameter for different values of N_e
(Monte-Carlo simulation for MAKET ANI installation)
S=[(3x6) - (1x2)]x4 m²
S=[(5x10) - (3x6)]x4 m²
S=[(7x14) - (5x10)]x4 m²
S=[(9x18) - (7x14)]x4 m²
S=[(11x22) - (9x18)]x4 m²
S=[(13x26) - (11x22)]x4 m²
Efficiency
Age
0
0.25
0.5
0.75
1
1.5
Log(N_e) = 4.699; 5.006; 5.313; 5.619; 5.926; 6.233; 6.540; 6.847
(from below upwards)

Figure 2:

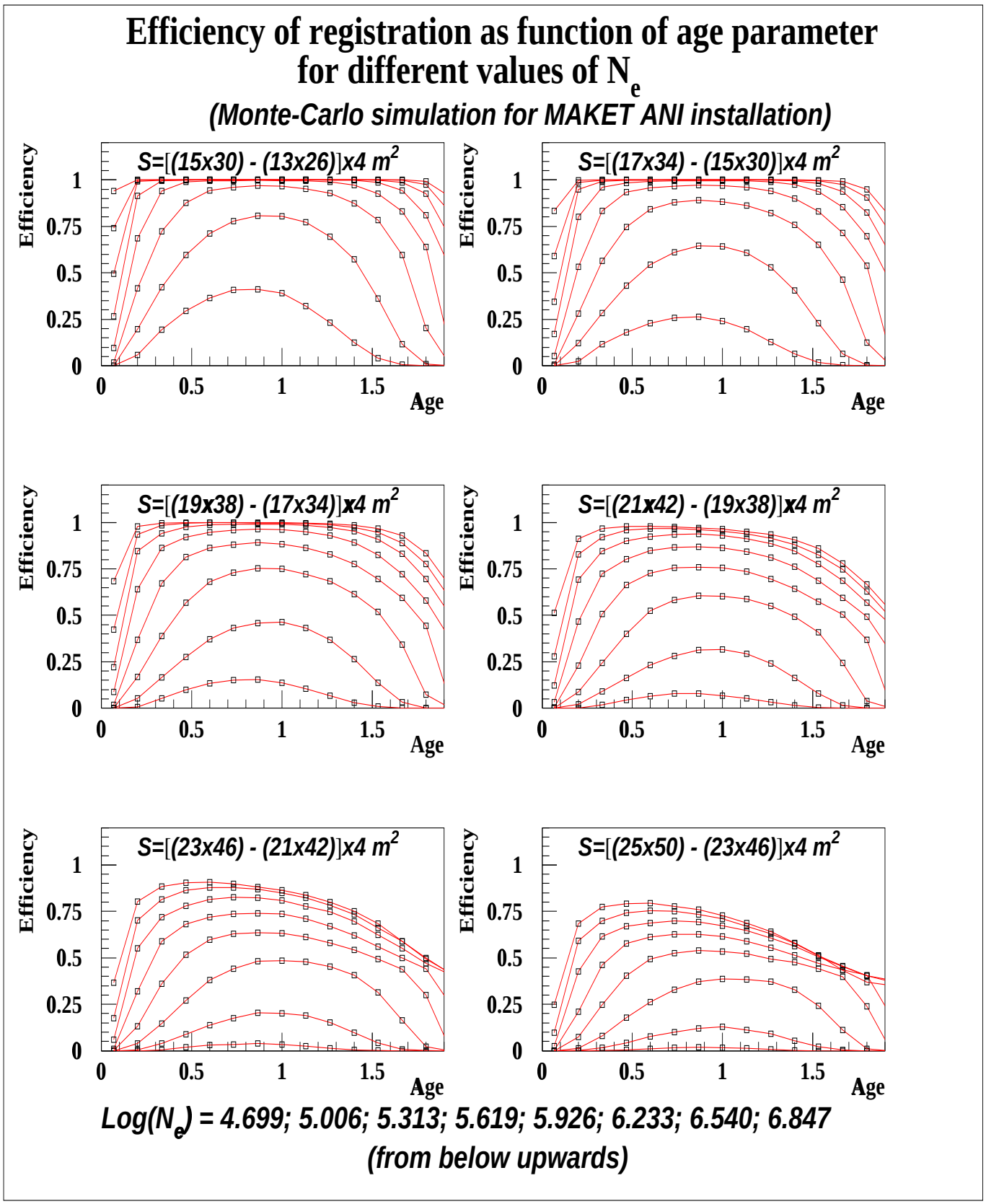
Efficiency of registration as function of age parameter for different values of N_e
(Monte-Carlo simulation for MAKET ANI installation)
S=[(15x30) - (13x26)]x4 m²
S=[(17x34) - (15x30)]x4 m²
S=[(19x38) - (17x34)]x4 m²
S=[(21x42) - (19x38)]x4 m²
S=[(23x46) - (21x42)]x4 m²
S=[(25x50) - (23x46)]x4 m²
Efficiency
Age
0
0.25
0.5
0.75
1
1.5
Log(N_e) = 4.699; 5.006; 5.313; 5.619; 5.926; 6.233; 6.540; 6.847
(from below upwards)

Figure 3:

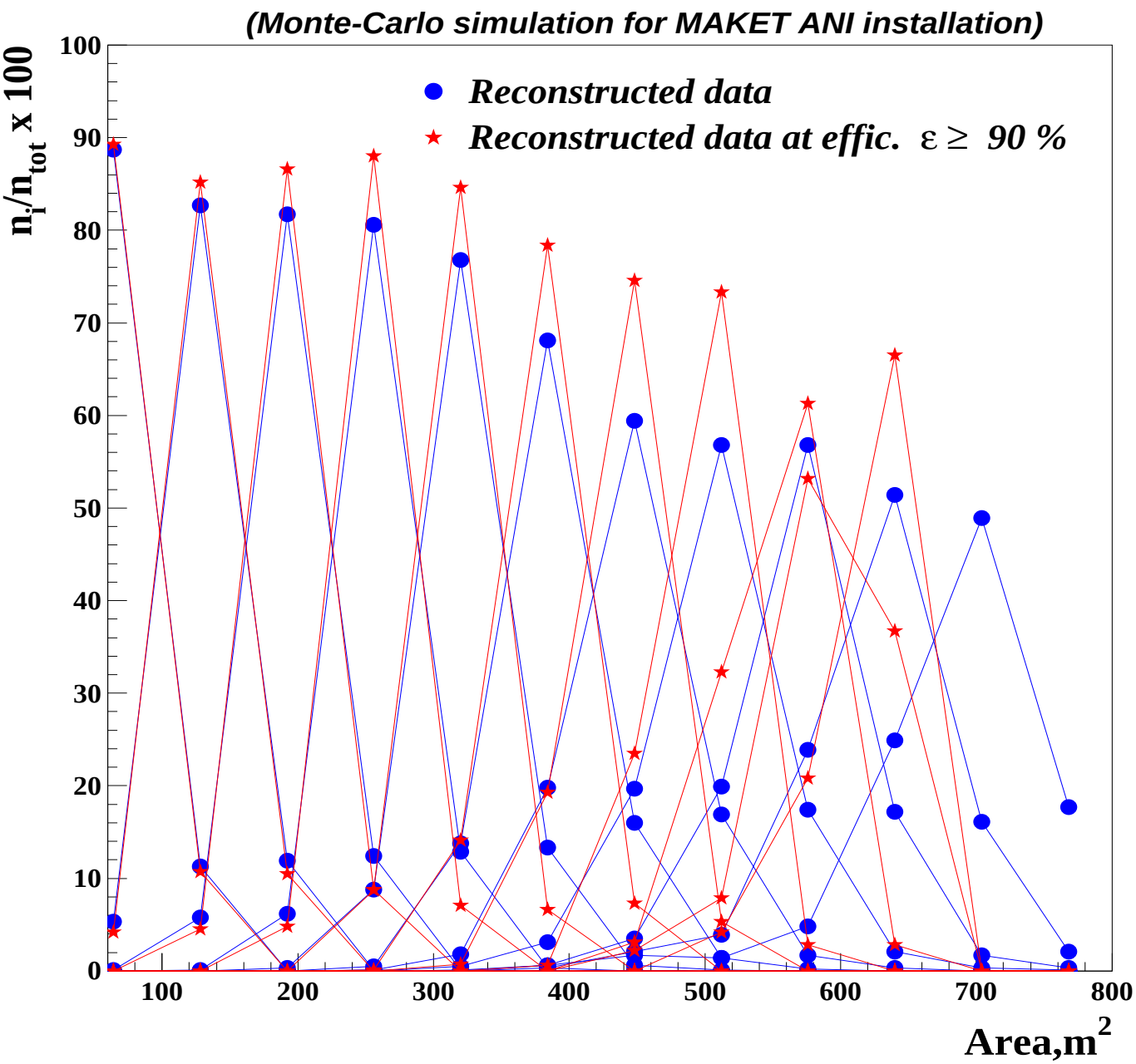
Distributions of events transfers for different belts
(Monte-Carlo simulation for MAKET ANI installation)
Reconstructed data
Reconstructed data at effic. ε ≥ 90 %
n_i/n_tot x 100
Area,m^2
0
10
20
30
40
50
60
70
80
90
100
100
200
300
400
500
600
700
800

Figure 4:

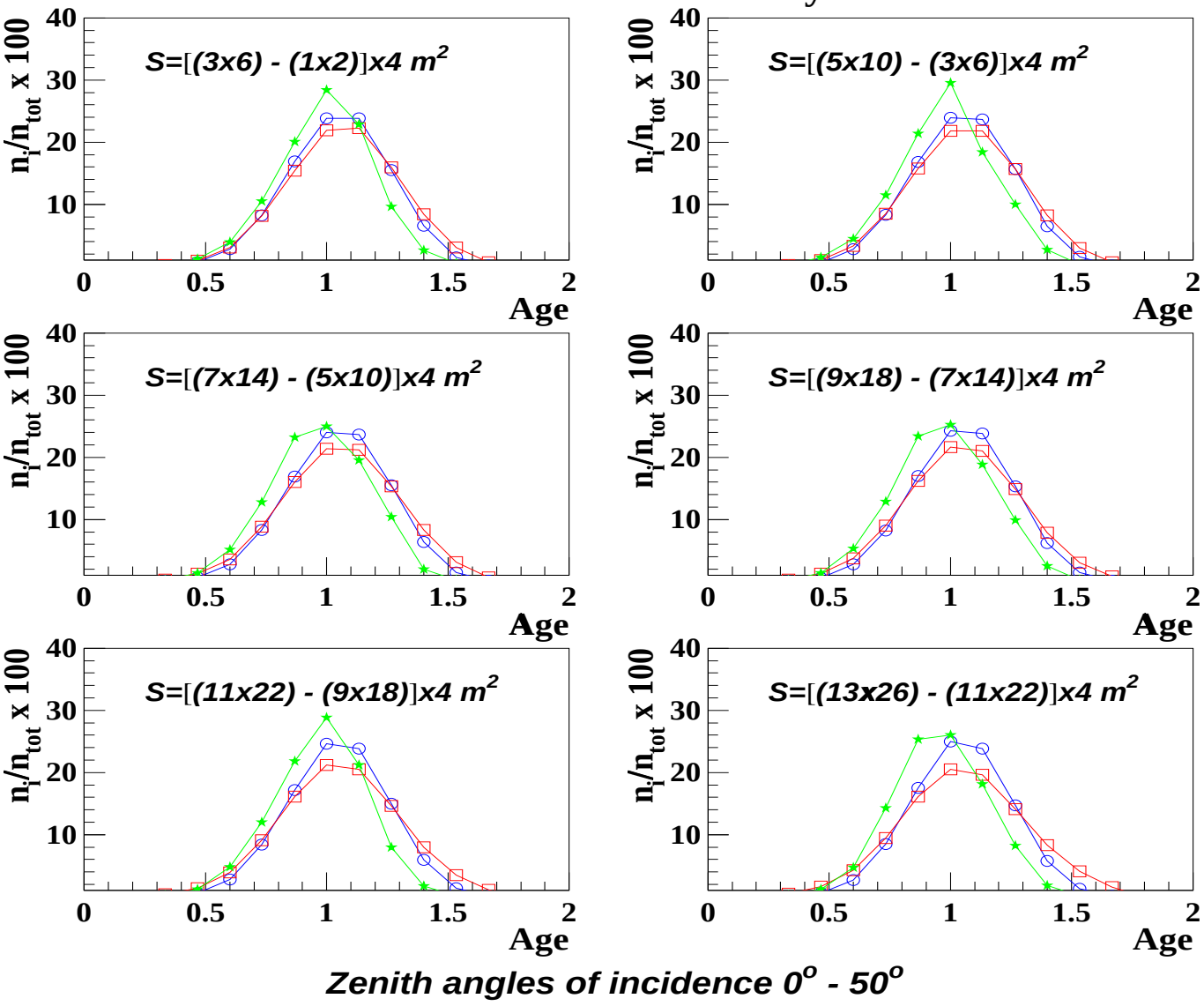
Age parameter distributions for different belts
(Monte-Carlo simulation for MAKET ANI installation)
M - C data
Reconstructed data
Reconstructed data at efficiency ε ≥ 90 %
S=[(3x6) - (1x2)]x4 m²
S=[(5x10) - (3x6)]x4 m²
S=[(7x14) - (5x10)]x4 m²
S=[(9x18) - (7x14)]x4 m²
S=[(11x22) - (9x18)]x4 m²
S=[(13x26) - (11x22)]x4 m²
n_i/n_tot x 100
Age
Zenith angles of incidence 0° - 50°

Figure 5:

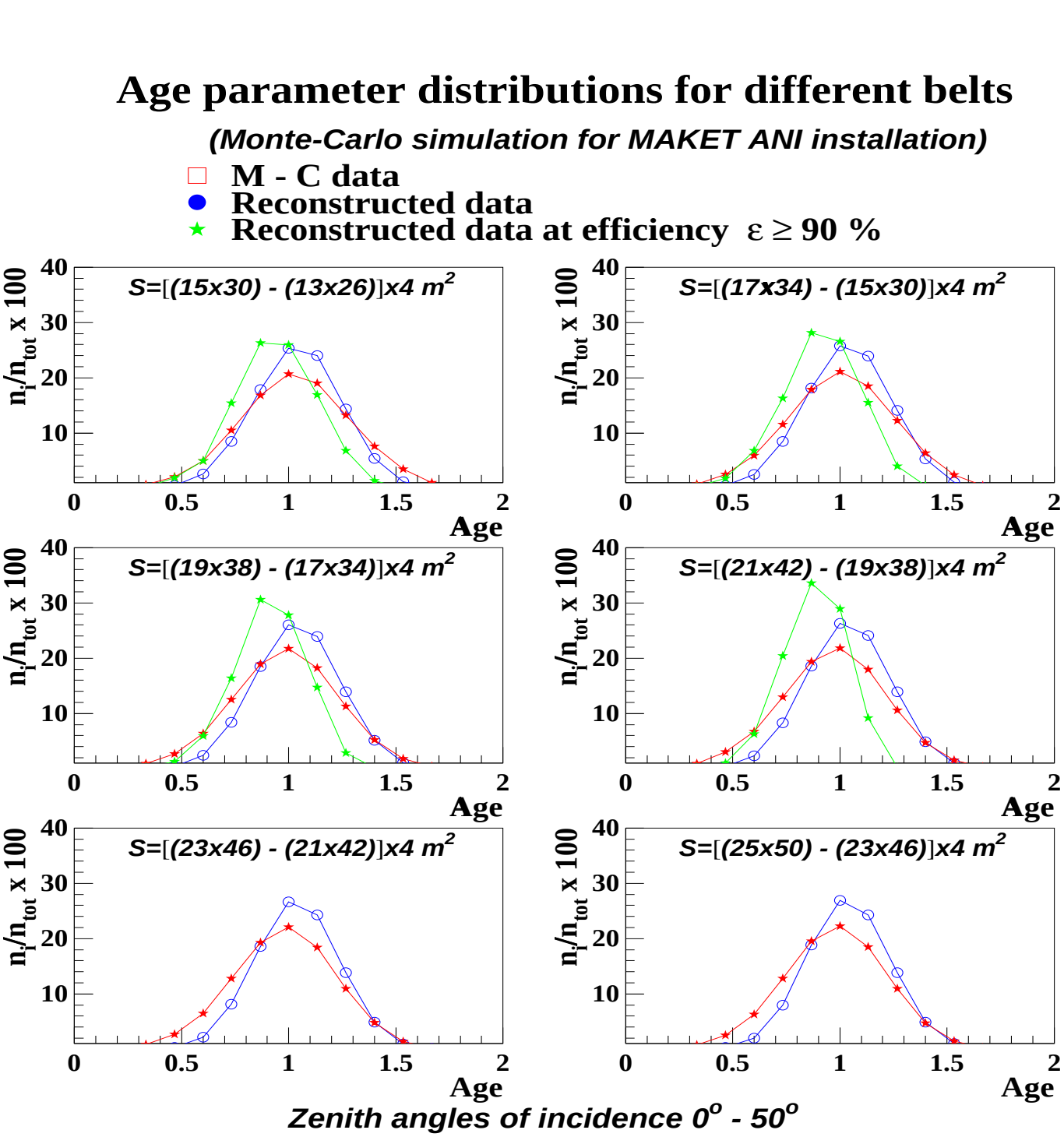
Age parameter distributions for different belts
(Monte-Carlo simulation for MAKET ANI installation)
M - C data
Reconstructed data
Reconstructed data at efficiency ε ≥ 90 %
S=[(15x30) - (13x26)]x4 m²
S=[(17x34) - (15x30)]x4 m²
S=[(19x38) - (17x34)]x4 m²
S=[(21x42) - (19x38)]x4 m²
S=[(23x46) - (21x42)]x4 m²
S=[(25x50) - (23x46)]x4 m²
n_i/n_tot x 100
Age
Zenith angles of incidence 0° - 50°

Figure 6:

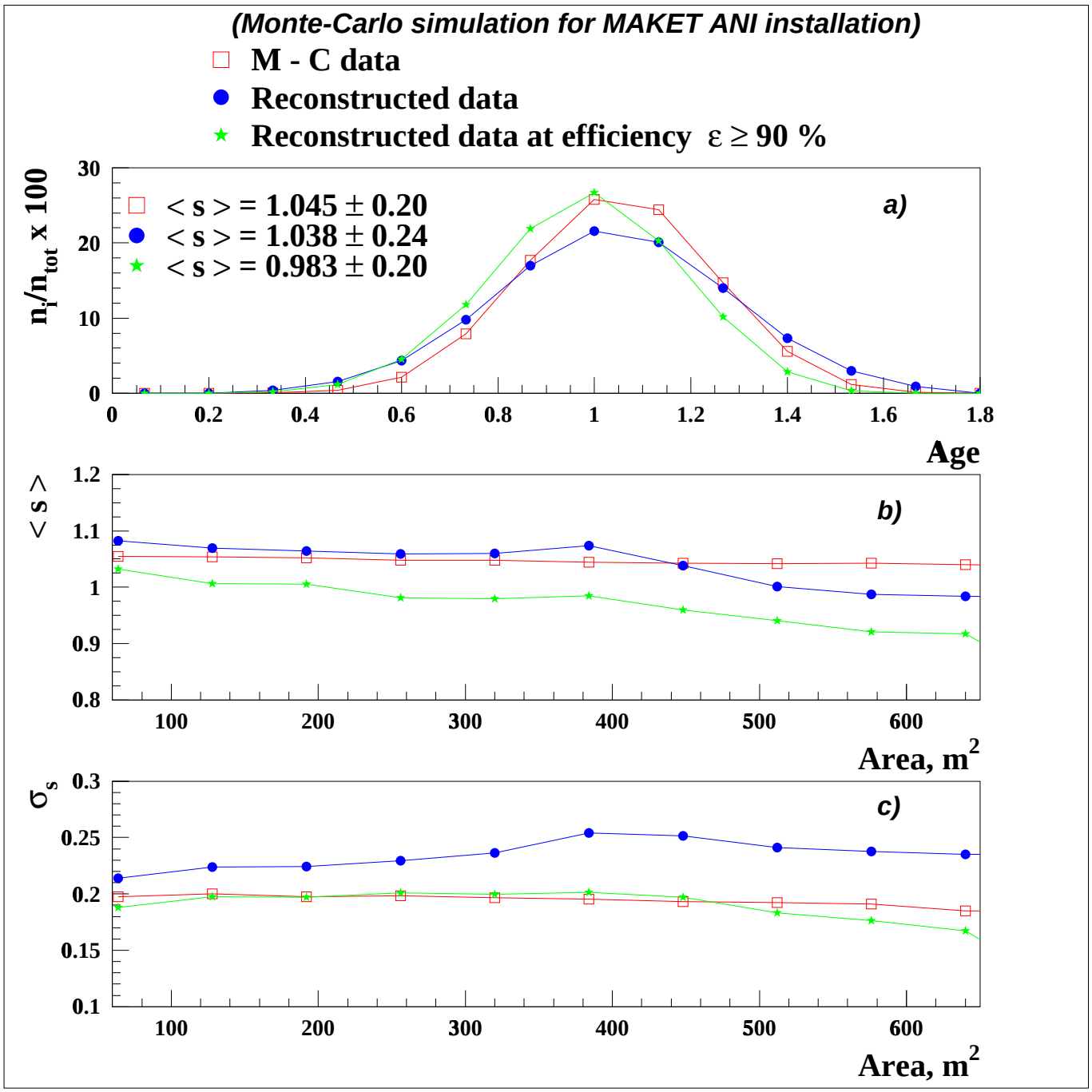
(Monte-Carlo simulation for MAKET ANI installation)
M - C data
Reconstructed data
Reconstructed data at efficiency ε ≥ 90 %
n_i/n_{tot} x 100
< s > = 1.045 ± 0.20
< s > = 1.038 ± 0.24
< s > = 0.983 ± 0.20
a)
Age
< s >
b)
Area, m^2
σ_s
c)
Area, m^2

Figure 7:

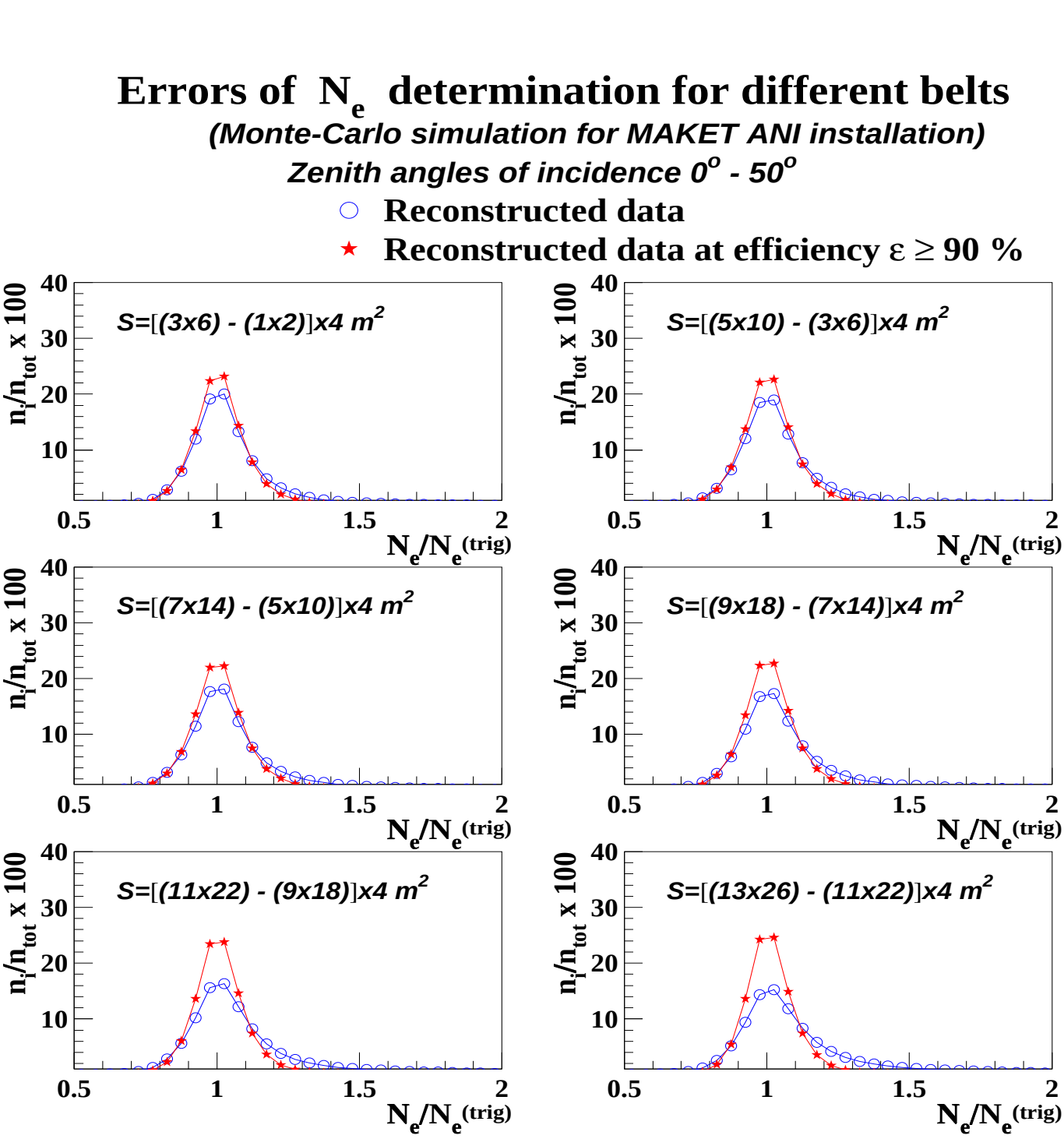
Errors of N_e determination for different belts
(Monte-Carlo simulation for MAKET ANI installation)
Zenith angles of incidence 0° - 50°
Reconstructed data
Reconstructed data at efficiency ε ≥ 90 %
S=[(3x6) - (1x2)]x4 m²
S=[(5x10) - (3x6)]x4 m²
S=[(7x14) - (5x10)]x4 m²
S=[(9x18) - (7x14)]x4 m²
S=[(11x22) - (9x18)]x4 m²
S=[(13x26) - (11x22)]x4 m²
n_i/n_{tot} x 100
$N_e/N_e^{(trig)}$
10
20
30
40
0.5
1
1.5
2

Figure 8:

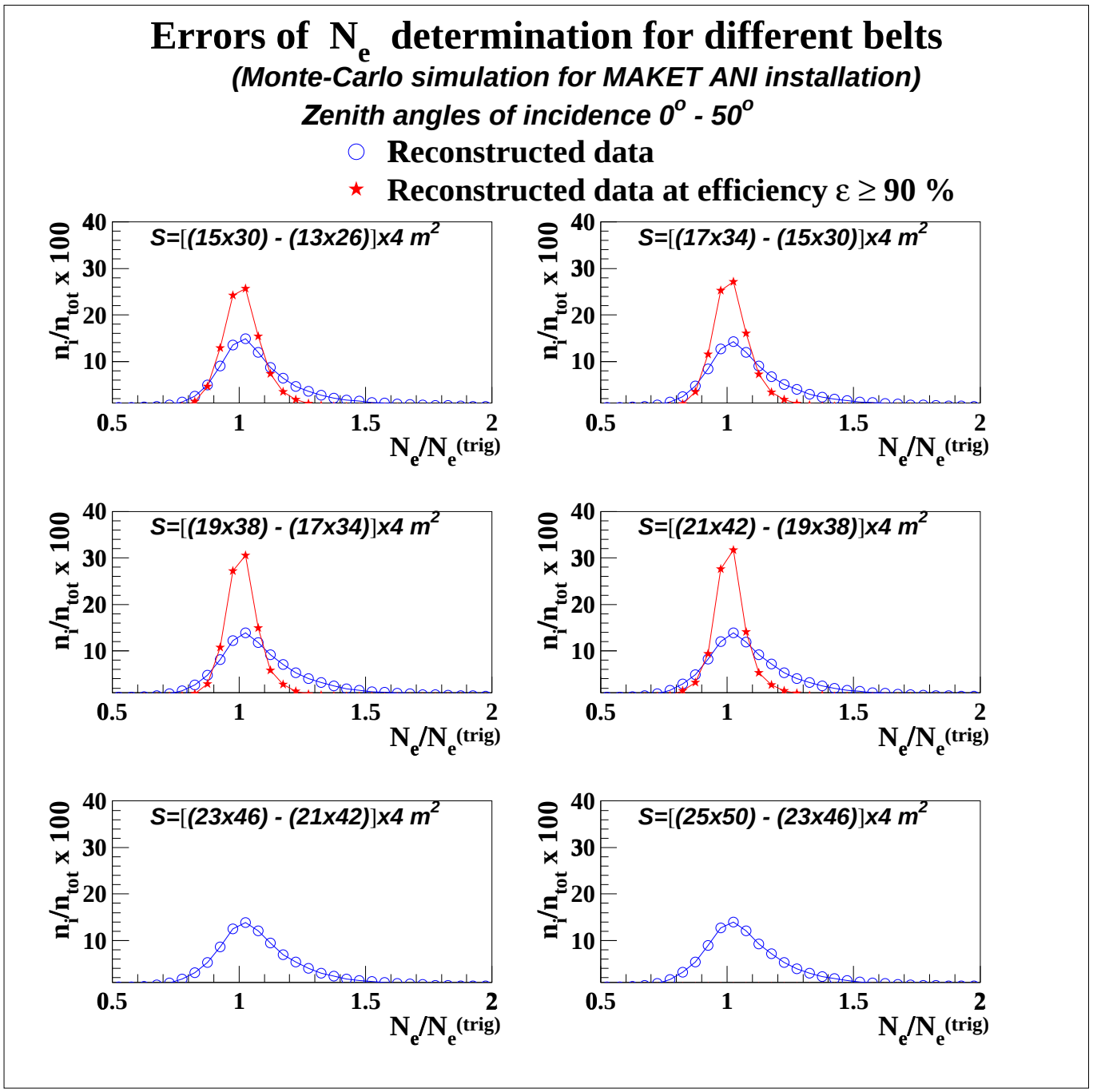
Errors of N_e determination for different belts
(Monte-Carlo simulation for MAKET ANI installation)
Zenith angles of incidence 0° - 50°
Reconstructed data
Reconstructed data at efficiency ε ≥ 90 %
S=[(15x30) - (13x26)]x4 m²
S=[(17x34) - (15x30)]x4 m²
S=[(19x38) - (17x34)]x4 m²
S=[(21x42) - (19x38)]x4 m²
S=[(23x46) - (21x42)]x4 m²
S=[(25x50) - (23x46)]x4 m²
n_i/n_{tot} x 100
$N_e/N_e^{(trig)}$

Figure 9:

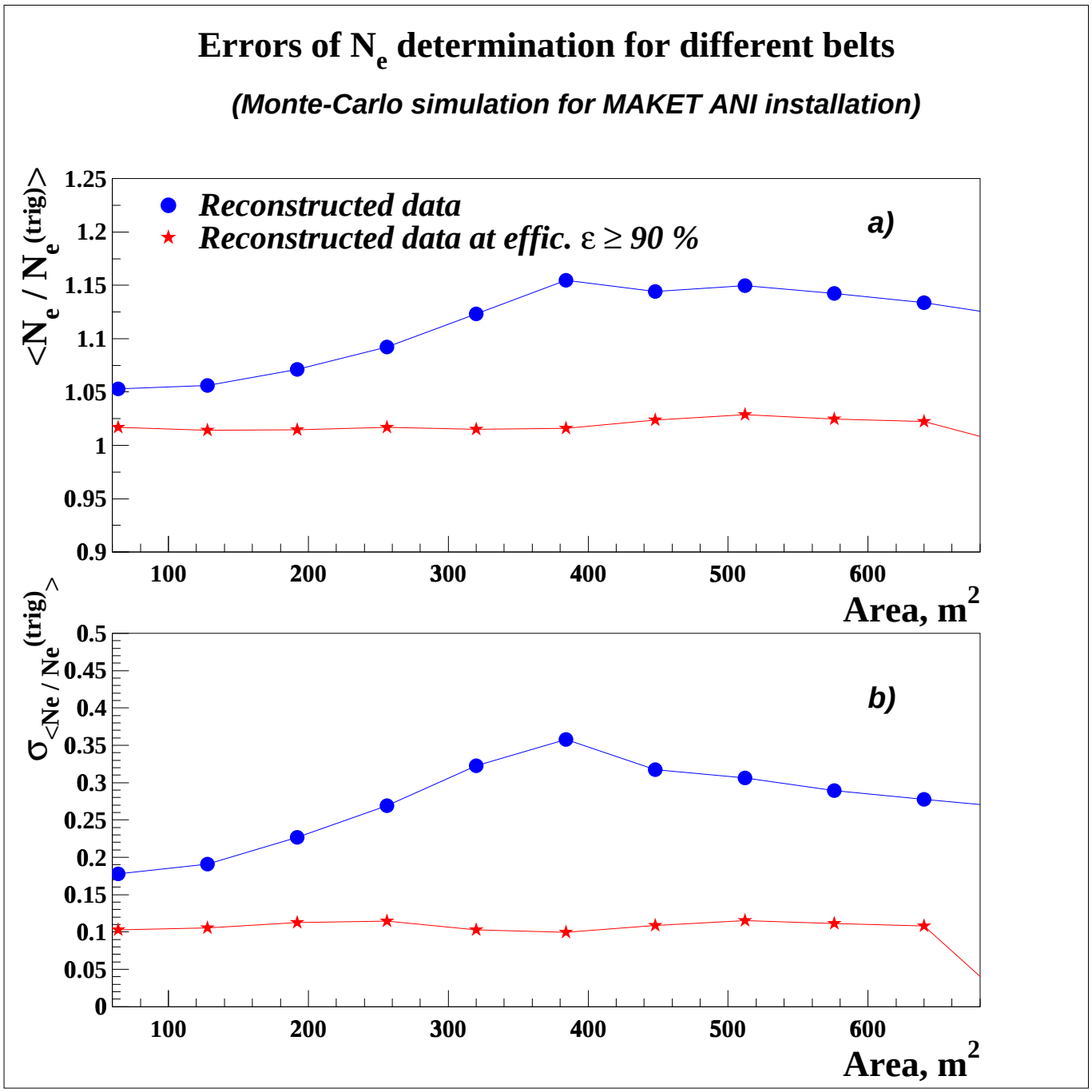
Errors of N_e determination for different belts
(Monte-Carlo simulation for MAKET ANI installation)
$<N_e / N_e(trig)>$
Reconstructed data
Reconstructed data at effic. ε ≥ 90 %
a)
1.25
1.2
1.15
1.1
1.05
1
0.95
0.9
100
200
300
400
500
600
Area, m^2
$\sigma_{<Ne / Ne(trig)>}$
b)
0.5
0.45
0.4
0.35
0.3
0.25
0.2
0.15
0.1
0.05
0
100
200
300
400
500
600
Area, m^2

Figure 10:

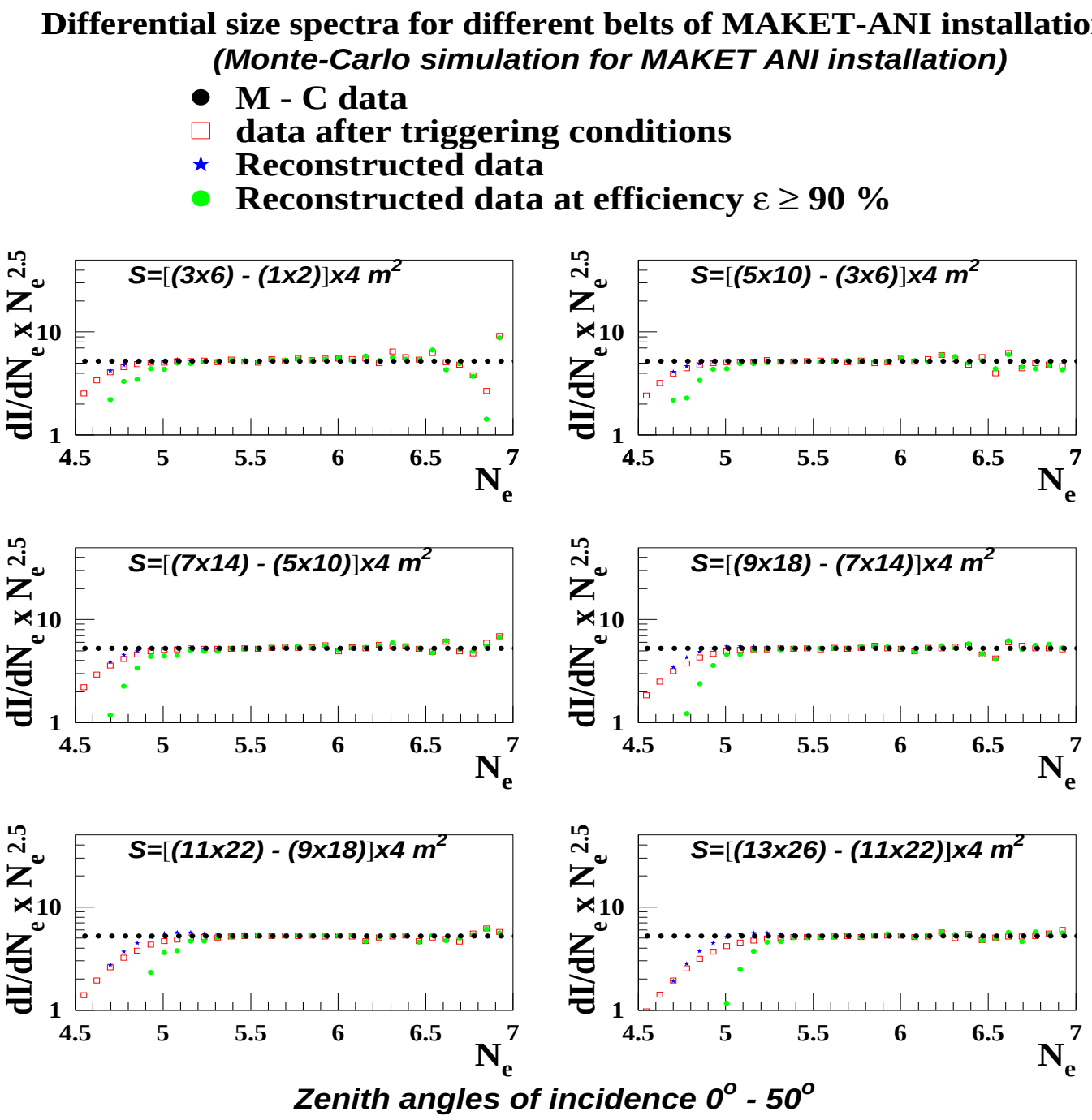
Differential size spectra for different belts of MAKET-ANI installation
(Monte-Carlo simulation for MAKET ANI installation)
M - C data
data after triggering conditions
Reconstructed data
Reconstructed data at efficiency ε ≥ 90 %
S=[(3x6) - (1x2)]x4 m2
S=[(5x10) - (3x6)]x4 m2
S=[(7x14) - (5x10)]x4 m2
S=[(9x18) - (7x14)]x4 m2
S=[(11x22) - (9x18)]x4 m2
S=[(13x26) - (11x22)]x4 m2
dI/dNe x Ne 2.5
Ne
Zenith angles of incidence 0o - 50o

Figure 11:

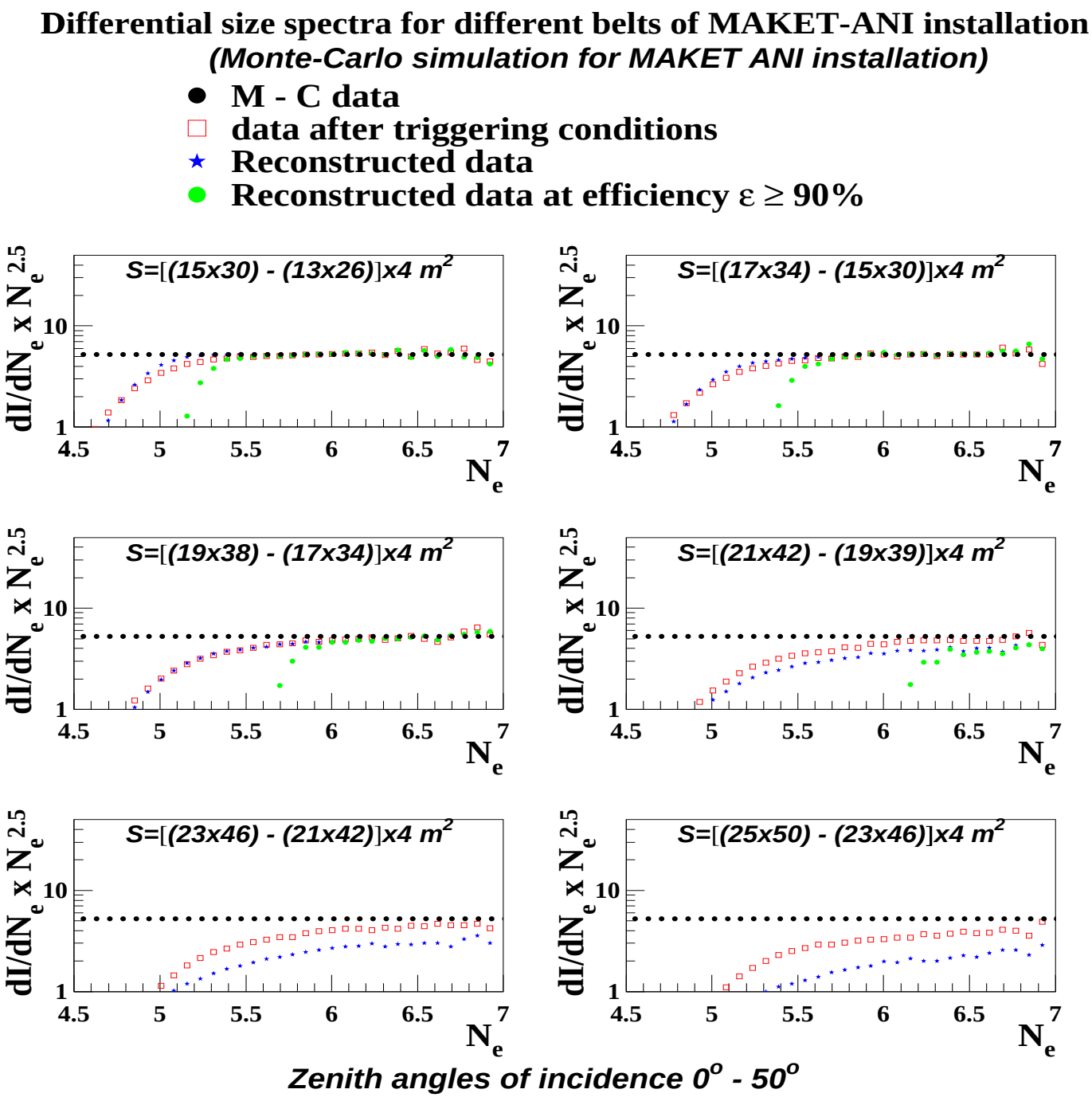
Differential size spectra for different belts of MAKET-ANI installation
(Monte-Carlo simulation for MAKET ANI installation)
M - C data
data after triggering conditions
Reconstructed data
Reconstructed data at efficiency ε ≥ 90%
S=[(15x30) - (13x26)]x4 m2
S=[(17x34) - (15x30)]x4 m2
S=[(19x38) - (17x34)]x4 m2
S=[(21x42) - (19x39)]x4 m2
S=[(23x46) - (21x42)]x4 m2
S=[(25x50) - (23x46)]x4 m2
dI/dNe x Ne2.5
Ne
Zenith angles of incidence 0o - 50o

Figure 12:

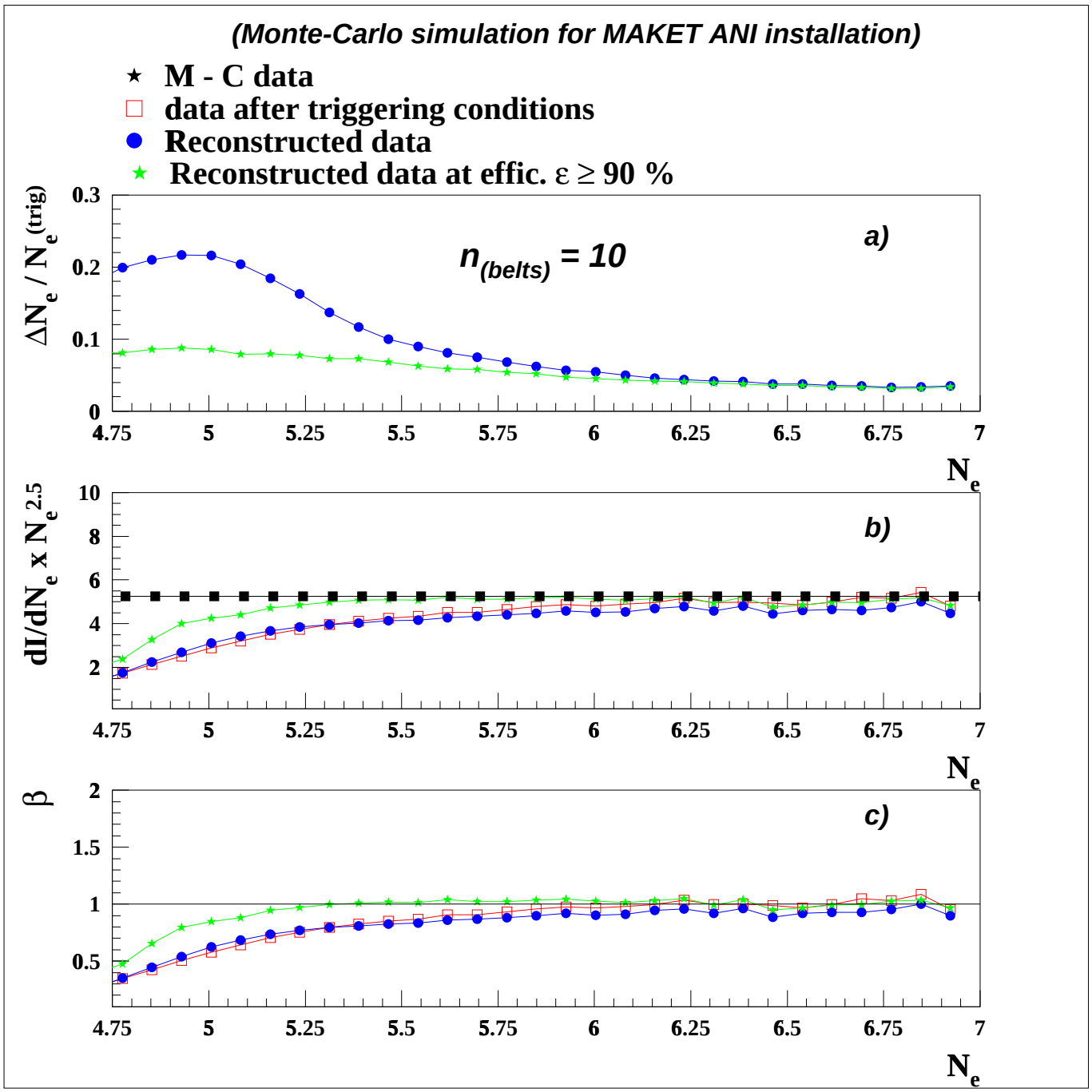
(Monte-Carlo simulation for MAKET ANI installation)
M - C data
data after triggering conditions
Reconstructed data
Reconstructed data at effic. ε ≥ 90 %
ΔNe / Ne (trig)
n(belts) = 10
a)
Ne
dI/dNe x Ne 2.5
b)
Ne
β
c)
Ne

Figure 13:

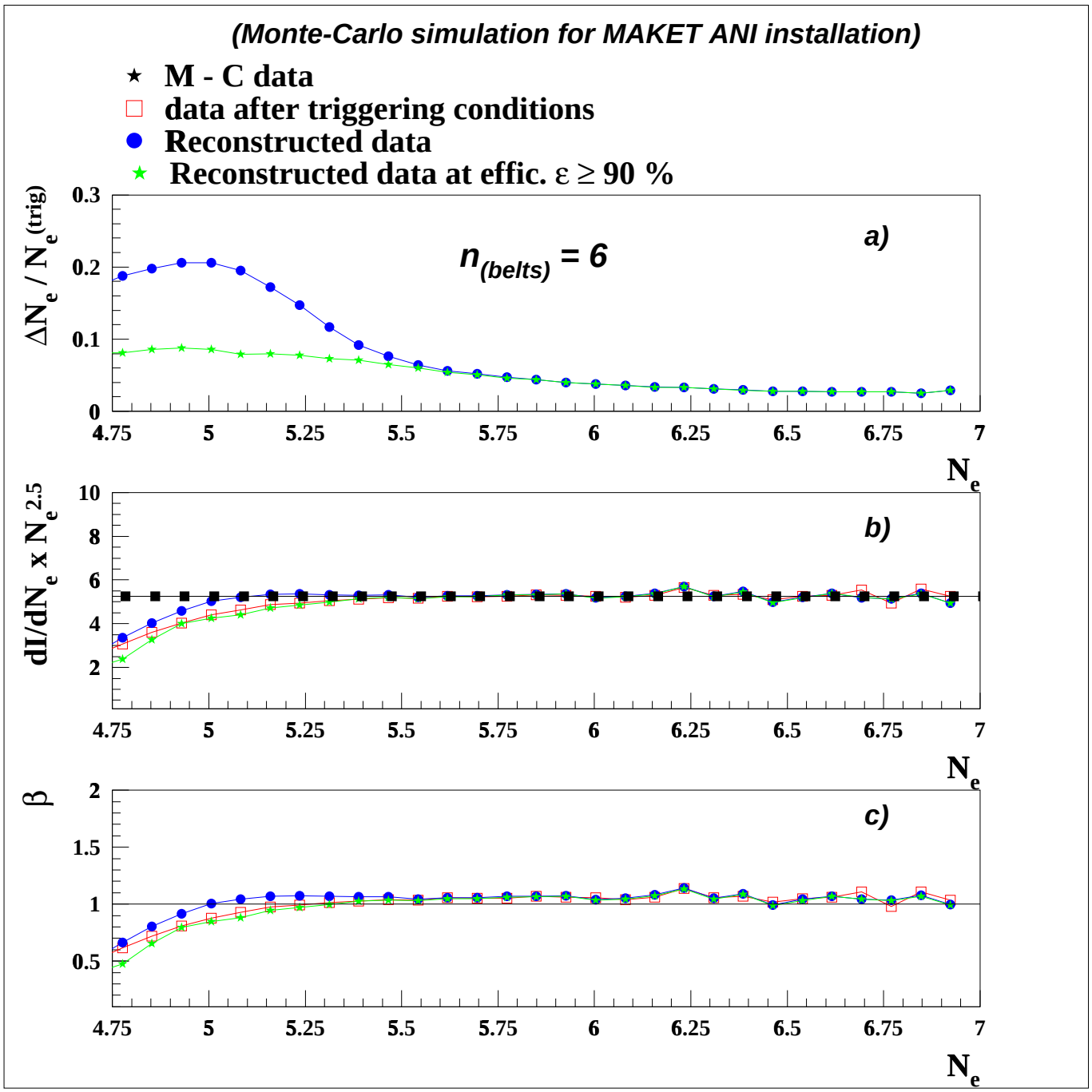
(Monte-Carlo simulation for MAKET ANI installation)
M - C data
data after triggering conditions
Reconstructed data
Reconstructed data at effic. ε ≥ 90 %
ΔNe / Ne (trig)
n(belts) = 6
a)
Ne
dI/dNe x Ne 2.5
b)
Ne
β
c)
Ne

Figure 14:

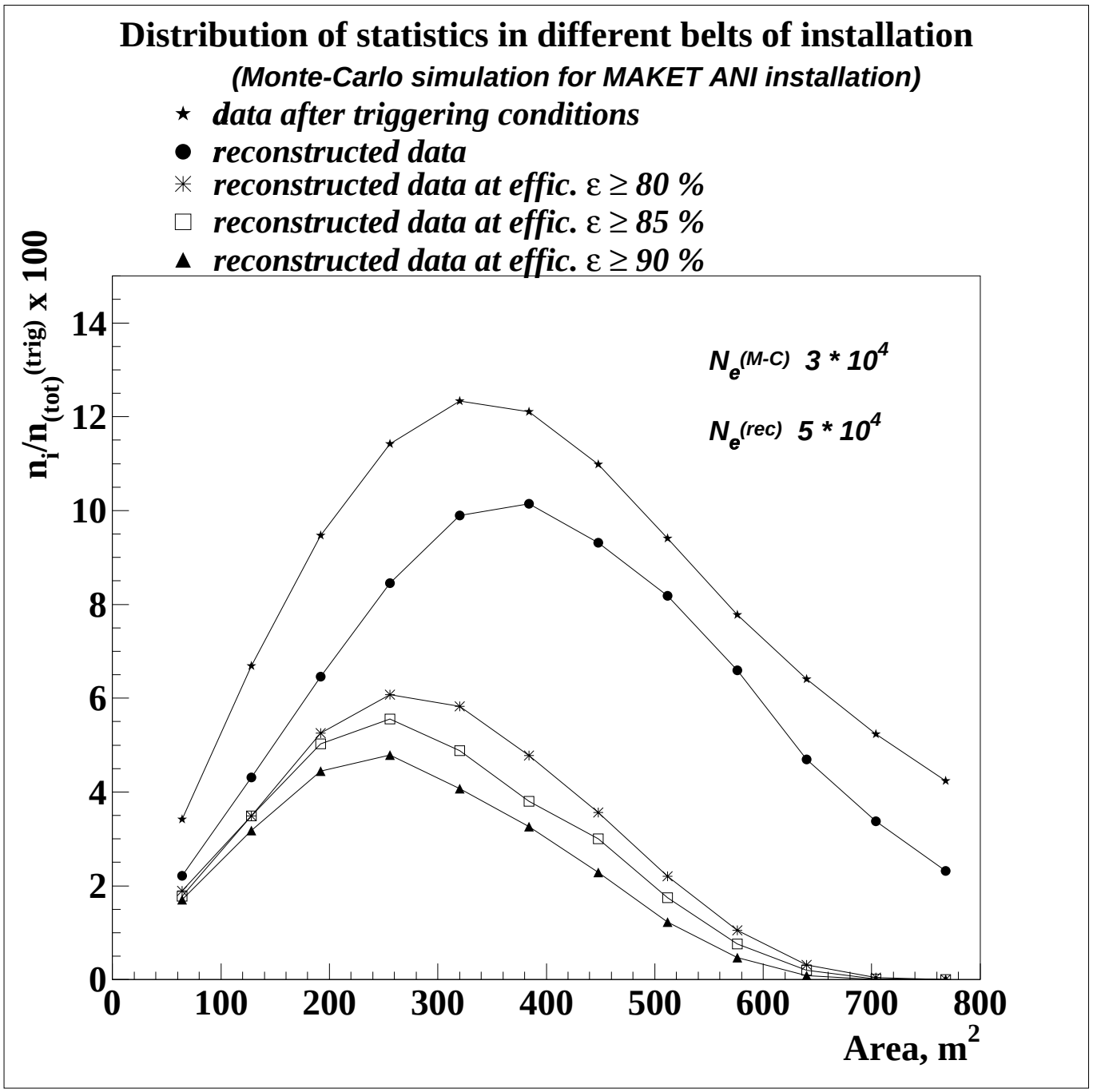
Distribution of statistics in different belts of installation
(Monte-Carlo simulation for MAKET ANI installation)
data after triggering conditions
reconstructed data
reconstructed data at effic. ε ≥ 80 %
reconstructed data at effic. ε ≥ 85 %
reconstructed data at effic. ε ≥ 90 %
$N_e^{(M-C)}$ 3 * 10^4
$N_e^{(rec)}$ 5 * 10^4
$n_i/n_{(tot)}^{(trig)}$ x 100
0
2
4
6
8
10
12
14
0
100
200
300
400
500
600
700
800
Area, m^2

Figure 15:

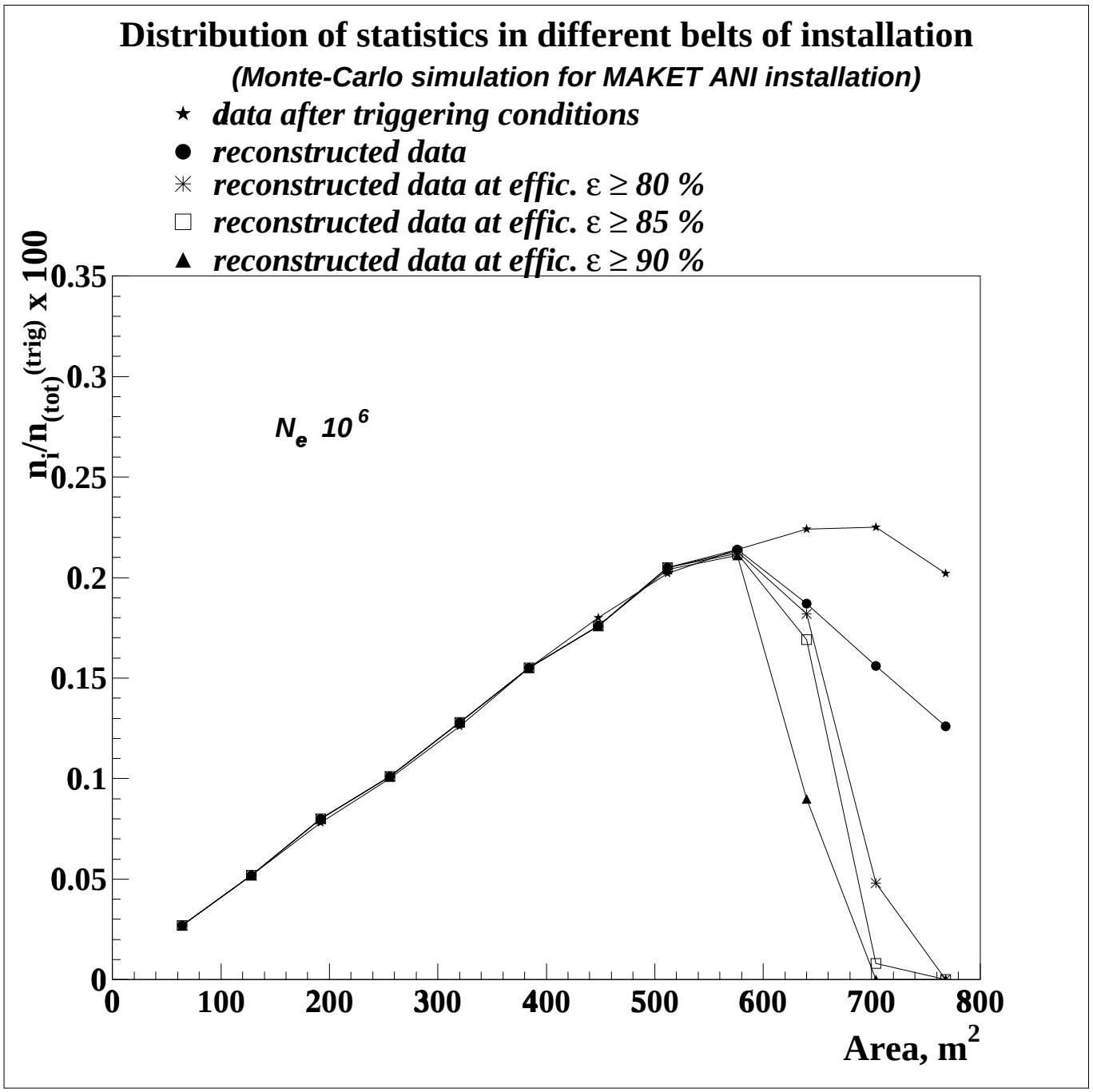
Distribution of statistics in different belts of installation
(Monte-Carlo simulation for MAKET ANI installation)
data after triggering conditions
reconstructed data
reconstructed data at effic. ε ≥ 80 %
reconstructed data at effic. ε ≥ 85 %
reconstructed data at effic. ε ≥ 90 %
$n_i/n_{(tot)}^{(trig)}$ x 100
N_e 10^6
0.35
0.3
0.25
0.2
0.15
0.1
0.05
0
0
100
200
300
400
500
600
700
800
Area, m^2

Figure 16: